Bio-Design and Manufacturing (2018) 1:146–156
https://doi.org/10.1007/s42242-018-0010-5

RESEARCH ARTICLE

Three-dimensional printing of β-tricalcium phosphate/calcium silicate composite scaffolds for bone tissue engineering

Yifan Dong[1,2] · Haibo Duan[4] · Naru Zhao[1,3] · Xiao Liu[1,2] · Yijuan Ma[4] · Xuetao Shi[1,3]

Received: 23 March 2018 / Accepted: 26 April 2018 / Published online: 21 May 2018

Abstract

Bioactive scaffolds with interconnected porous structures are essential for guiding cell growth and new bone formation. In this work, we successfully fabricated three-dimensional (3D) porous β-tricalcium phosphate (β-TCP)/calcium silicate (CS) composite scaffolds with different ratios by 3D printing technique and further investigated the physiochemical properties, in vitro apatite mineralization properties and degradability of porous β-TCP/CS scaffolds. Moreover, a series of in vitro cell experiments including the attachment, proliferation and osteogenic differentiation of mouse bone marrow stromal cells were conducted to testify their biological performances. The results showed that 3D printed β-TCP/CS scaffolds possessed of controllable internal porous structures and external shape. Furthermore, the introduction of CS decreased the shrinkage of scaffolds and improved the in vitro apatite formation activity and degradation rate. Meanwhile, compared with pure β-TCP scaffold, the β-TCP/CS composite scaffolds were more conducive to promote cell adhesion, spread and osteogenesis differentiation. However, when the content of CS was increased to 45%, the ions dissolution rate of the composite scaffolds was so high that leaded to the increase in pH value, which inhibited the proliferation of cells. Our results suggested that the introduction of appropriate CS into β-TCP bioceramic is an effective strategy to prepare bioactive 3D printed bioceramic scaffolds for hard tissue regeneration.

Keywords 3D printing · β-Tricalcium phosphate/calcium silicate · Osteogenesis differentiation · Tissue regeneration

Introduction

To meet clinical requirements, three-dimensional (3D) porous bone repair scaffolds are required to have good pore interconnectivity, excellent bioactivity, controlled biodegradability, and sufficient mechanical strength. β-tricalcium phosphate (β-$Ca_3(PO_4)_2$, β-TCP) has been widely used in clinical as bone defect repair materials due to its excellent biocompatibility, osteoconductivity and its chemical composition similar to human biological apatite [1–3]. However, the β-TCP also has the defects of slow bone formation and degradation rate in vivo, which restricted its wide application in clinic [1,3]. In recent years, bioactive ceramics containing silicon have received extensive attention due to their outstanding biological activity and excellent osteogenic and angiogenic activities [4–6]. It has been reported that calcium silicate (CS) can upregulate the expression of osteogenesis-related genes and has an important effect on bone formation [7,8]. However, the rapid degradation of CS may lead to decline in mechanical strength after the scaffold implantation, which cannot meet the mechanical requirements of early bone formation. Thus, the β-TCP/CS composites have been designed, and the studies have demonstrated that the β-TCP/CS composites not only showed a controllable the degradation rate but also stimulated osteogenic differentiation of osteoclasts [9,10]. However, most of these studies

Yifan Dong and Haibo Duan have contributed equally to this work.

Electronic supplementary material The online version of this article (https://doi.org/10.1007/s42242-018-0010-5) contains supplementary material, which is available to authorized users.

✉ Naru Zhao
nrzhao@scut.edu.cn

1 School of Materials Science and Engineering, South China University of Technology, Guangzhou 510641, China

2 National Engineering Research Centre for Tissue Restoration and Reconstruction, Guangzhou 510006, China

3 Guangdong Province Key Laboratory of Biomedical Engineering, South China University of Technology, Guangzhou 510006, China

4 South China Institute of Collaborative Innovation, Dongguan, China

focused on the extracts or compact pellets of β-TCP/CS composites, and did not discussed the performance of the 3D porous composite scaffold.

Nowadays, various techniques have been developed for preparing 3D porous bioceramic scaffolds including porogen techniques, gas foaming techniques, solvent casting, polyurethane foam templating and freeze-drying [11–15]. However, these traditional methods cannot precisely regulate the internal pore structure of the scaffolds, which will directly affect the mechanical strength of the prepared scaffolds as well as the formation and growth of tissue. 3D printing using concentrated colloidal slurry offers a new approach for creating 3D periodic bioceramic scaffolds [16–18].

Herein, β-TCP/CS composite porous scaffolds with various β-TCP/CS ratios and accurately controlled 3D structure and pore size were prepared by 3D printing technique. The physicochemical properties, in vitro apatite formation abilities and degradability of porous β-TCP/CS scaffolds were investigated, and their effect on mouse bone marrow stem cells (BMSCs) growth and osteogenic differentiation was further investigated.

Materials and methods

Synthesis of powders

β-TCP powders were synthesized by a chemical precipitation method as reported previously [19]. CS powders were prepared by a precipitation method using $Ca(NO_3)_2{\cdot}4H_2O$ (Guangzhou Chemical Co., China) as calcium source and $Na_2SiO_3{\cdot}9H_2O$ (Guangzhou Chemical Co., China) as silicon source. Briefly, $Ca(NO_3)_2{\cdot}4H_2O$ was dissolved in deionized water (0.5 M), adding dispersant polyethylene glycol (PEG-6000, Guangzhou Chemical Co., China) with the mass of 0.5 wt%. 0.5 M $Na_2SiO_3{\cdot}9H_2O$ solution was added dropwise to the $Ca(NO_3)_2{\cdot}4H_2O$ solution and stirred to produce a white precipitate. After stirring for 2 h, the precipitate was separated by centrifugation, washed three times with distilled water, and washed twice with absolute ethanol. Finally, the precipitate was dried at 60 °C for 48 h and then calcined at 1100 °C for 3 h to obtain CS powders.

Fabrication of β-TCP/CS scaffolds by 3D printing

The 3D printing device (3D-Bioplotter^{TM} system) was developed by envisionTEC GmbH (Brüsseler, Germany). The printing slurry was prepared by adding 45 vol% β-TCP/CS into a mixture of distilled water and glycerol (weight ratio 7:3); then ammonium polyacrylate (PAA-NH_4, Adamas, China) (1.5 wt%) was added into the system as a dispersant. pH was adjusted to 9 using ammonia water (1 mol/L) and hydrochloric acid (1 mol/L). The β-TCP/CS powders were added to the QM-BP planetary ball mill (Nanjing Nanda Instrument Plant, China) and milled for 8–10 h to insure the homogeneity of the slurry. Hydroxypropylmethyl cellulose (4000 Pa s, Aladdin, USA) was used to improve the viscosity, and three drops of octanol were added to eliminate foams of the slurry. The prepared slurry was loaded into printing cartridges and aged to use. Different proportions of CS and TCP powders were mixed up to obtain a series ratio of β-TCP/CS slurries. β-TCP/CS scaffolds were fabricated by 3D-Bioplotter via a dosing pressure of 3–6 bar and a printing speed of 8 mm s^{-1}. According to the results of the previous researches [11,14], the scaffold structure of this study was designed as follows: the size of the scaffold was Φ12 × 4 mm via 3D CAD software SolidWorks; the fiber diameter of the scaffold was 400 μm using 410 μm tapered tip (Nordson EFD, USA); the inner pore diameter of the scaffold was 400 μm provided by 3D-Bioplotter system. The preformed scaffolds were dried at room temperature for 48 h and then calcined at 1100 °C for 3 h to obtain β-TCP/CS scaffolds. The scaffolds prepared with four different CS mass percentages of CS/TCP slurries (0, 5, 15 and 45 wt% CS) were sequentially labeled as β-TCP, 5, 15 and 45% CS.

Characterization of β-TCP/CS scaffolds

The microstructure and phase compositions of the as-synthesized powers and the β-TCP/CS scaffolds were characterized by scanning electron microscopy (SEM, MERLIN Compact, Carl Zeiss, Germany) and X-ray diffraction (XRD; D8 Advance, Bruker, Germany) with Cu Ka radiation. The pore connectivity and inner porous structure of the β-TCP/CS scaffolds were observed by micro-CT (XTV160H, Nikon, Japan). The linear shrinkage of the β-TCP/CS scaffolds was calculated from the sizes of the scaffolds before and after sintering. The compressive strength and Young's modulus of the β-TCP/CS scaffolds (Ø 8 × 16 mm) were tested using a computer-controlled universal testing machine (Instron 5960, USA) at a cross-head speed of 0.5 mm min^{-1}. Four samples were used for replicates to test linear shrinkage and mechanical strength.

Mineralization of β-TCP/CS scaffolds in simulated body fluid (SBF)

Simulated body fluids (SBF), which ion concentrations were close to those of human blood plasma, was prepared following the method described by Kokubo et al. [20]. The β-TCP/CS scaffolds were soaked in SBF ($V_{SBF}/M_{scaffolds}$: 100 mL g^{-1}) at 37 °C for 1 and 3 days. Three samples were used for repeated experiments. After soaking for the preset time, the scaffolds were removed from SBF, rinsed 3 times with distilled water and acetone, respectively, and then dried at 60 °C overnight. Apatite mineralization of scaffolds

was observed by SEM and energy-dispersive spectrometry (EDS).

Degradation behavior of β-TCP/CS scaffolds

The degradability of β-TCP/CS scaffolds was evaluated by soaking them in Tris-HCl buffered solution (pH = 7.40) ($V_{Tris\text{-}HCl}/M_{scaffolds}$: 100 mL g^{-1}) for 1, 7, 14 and 21 days in a shaker at 37 °C. The pH value of the solution was measured with an electrolyte-type pH meter before refreshed the solution every 2 days. The scaffolds were collected from Tris-HCl buffered solution after the scheduled time, rinsed 3 times with deionized water and dried at 120 °C overnight, the final weight of each scaffold was measured accurately. Five samples were used for replicates of this experiment. The degradability of the β-TCP/CS scaffolds was expressed as the weight loss percentage of the initial weight.

The osteogenic activity of mBMSCs in β-TCP/CS scaffolds

Attachment and proliferation

In this experiment, mouse mesenchymal stem cells (mBMSCs, CRL-12424, ATCC, USA) were cultured in high glucose Dulbecco's modified Eagle's medium (H-DMEM, Gibco, USA) with 10% fetal bovine serum (FBS, Gibco, USA) and 1% penicillin/ streptomycin (Gibco) at 37 °C in a humidified 5% CO_2 atmosphere. Medium was replaced every 2 days. The 50 ul cell suspensions (1×10^6 cells per mL) were seeded into scaffolds in 24-well culture plates and allowed to attach for 1 h before 1 mL culture medium was added in an incubator at 37 °C under 5% CO_2. The culture medium was renewed every 2 days.

The cell adhesion and spreading on different β-TCP/CS scaffolds were observed using SEM and laser scanning confocal microscopy (Leica TCS SP5, Germany) after 1 and 4 days of cell culture. The scaffolds were removed from the culture wells after incubating for 1 day, rinsed 3 times with PBS and fixed with 2.5% glutaraldehyde for 60 min, then washed with PBS and dehydrated sequentially in graded ethanol (30, 50, 70, 80, 90, 95 and 100% (v/v)) at preset intervals. Finally, the scaffolds were air-dried and sputter-coated with gold for SEM observation. After 4 days of cell culture, the scaffolds were rinsed with PBS and fixed by 4% paraformaldehyde, then washed twice with PBS, permeabilized with 0.1% Triton X-100 in PBS for 5 min and blocked with 1% BSA (Sigma) in PBS for 10 min. After washing with PBS, Cytoskeleton of cells were stained for 1 h at room temperature using phalloidin-FITC (AAT, USA), cell nuclei was stained using DAPI (Beyitime, China) for 5 min, and the scaffolds were washed 3 times with PBS to reduce the non-specific binding. The staining images were visualized using laser scanning confocal microscope.

To assess proliferation of cells on the scaffolds, the cell counting Kit-8 (CCK-8, Dojindo, Japan) was used according to the manufacturer's instructions. After 1, 4 and 7 days of cell culture, the scaffolds were incubated in 300 ul CCK-8 working solution ($V_{CCK\text{-}8}/V_{DMEM}$ = 1:9) at 37 °C for 1 h after the media was removed. Then, 100 ul supernatant was transferred to a 96-well plate and the OD value at 450 nm was measured using a microplate reader (Thermo 3001, USA).

Cell cytotoxicity was evaluated by live/dead stain kit (Dojindo, Kumamoto, Japan). Briefly, after 3 days of cell culture, the scaffolds were washed three times with PBS and stained by PBS containing calcein-AM (1 mM) and PI (3 mM) for 30 min in the dark at 37 °C under 5% CO_2. Scaffolds were washed two times with PBS after staining and observed by the fluorescence microscopy (Eclipse Ti-U, Nikon, Japan).

Bone-related gene expression

After 5 and 10 days of cell culture, the osteoblastic gene expression of ALP, Collagen-I, Runx-2 and OPN was detected by real-time polymerase chain reaction (RT-PCR). In short, the Trizol reagent was used to isolate total RNA of cells (Invitrogen, Carlsbad, CA). The reverse transcription reagents kit was used to synthesize cDNA from the isolated RNA (Script™ cDNA Synthesis Kit, Bio-Rad, USA) according to the manufacturer's protocol. The QuantStudio™ 6 Flex system (Life Technologies, USA) and the SYBR green system (Invitrogen, USA) were used for RT-PCR. The housekeeping gene GAPDH was selected as control to normalize the expression of each target gene, and quantification was based on the cycle threshold (Ct) values using the ΔΔCt method. The primer sequences used for qRT-PCR in this study are listed in Table 1.

Statistical analysis

Dates were expressed as the means ± SD from three separate experiments, and significant differences were examined using the *t* test. A value of $^*P < 0.05$ was considered statistically significant.

Results and discussion

Characterization of 3D printed β-TCP/CS scaffolds

Many studies have shown that three-dimensional connected porous scaffolds not only provide a place for cell growth and differentiation but also provide pathways for the transportation of nutrients and metabolites. In this study, porous

Table 1 Validated primer sequences for real-time PCR

Gene	Direction	Sequence (5′-3′)
GAPDH	Forward	TGGATGGCCCCTCCGGGAAA
	Reverse	AGTGGGGACACGGAAGGCCA
Runx2	Forward	CACTGGCGGTGCAACAAGA
	Reverse	TTTCATAACAGCGGAGGCATTTC
ALP	Forward	TGCCTACTTGTGTGGCGTGAA
	Reverse	TCACCCGAGTGGTAGTCACAATG
Collagen-I	Forward	ATGCCGCGACCTCAAGATG
	Reverse	TGAGGCACAGACGGCTGAGTA
OPN	Forward	TGCAAACACCGTTGTAACCAAAAGC
	Reverse	TCTTTACGTTTGCCGGTGACGT

bioceramic scaffolds were prepared by 3D printing technology, the pore structure and pore connectivity can be accurately controlled. Figure 1 shows optical micrograph and micro-CT three-dimensional images as well as SEM images of β-TCP/CS porous scaffolds by 3D printing. It can be seen that the prepared scaffolds had controllable shapes (from cubic to cylinder), pore sizes (from millimeters to micrometers) and porosities (Fig. 1a). Micro-CT three-dimensional reconstruction analysis revealed that the scaffolds via 3D printing possessed of tailored geometry (Fig. 1b) and interconnected 3D structure (Fig. 1d). The macroscopic pores displayed regular and uniform square structures (Fig. 1c).

SEM analysis revealed that all the scaffolds possessed of highly regular and interconnected macro pores. The pore sizes and strand distance were approximately 400 μm, which were consistent with the setting parameters for the fabrication of the scaffolds. Some micro-pores, generally in the sizes of 1–2 μm, were distributed across the filaments (Fig. S-a, c, e, g, Supplementary information), which may be caused by the evaporation of moisture and organics in the process of sintering. It was believed that the controllable pore structures and pore sizes of the prepared scaffolds could benefit cell and tissue ingrowth as well as delivery of nutrients and metabolic wastes according to the previous publication [21]. All these above results demonstrated that the constructed β-TCP/CS scaffold possessed of a controllable pore structure and pore size, which contribute to achieve personalized customization.

The crystal phases of β-TCP powders and CS powders prepared by chemical precipitation method after calcination at 800 and 1100 °C for 3 h are presented in Fig. 2a, b. All diffraction peaks correspond to the characteristic peaks of the standard card (TCP:JCPDS NO. 09-0169, CS:JCPDS No. 27-0088), and no impurity peaks were detected, indicating that the synthesised powders are β-TCP and β-CS with high purity and good crystallinity. The crystal phases of β-TCP/CS scaffolds at 1100 °C for 3 h can be seen in Fig. 2c, the results showed that the composites were composed of CS and β-TCP phases and no peaks of impurities were identified, which suggested that there was no interaction between the β-TCP and the CS.

Shrinkage and mechanical properties of 3D printed β-TCP/CS scaffolds

For ceramic materials, the shrinkage is a very important indicator, which will directly affect the matching degree between the implant and the defective parts. Therefore, it is of great practical significance to study the effect of different CS contents on the shrinkage of scaffolds to achieve accurate customization. The linear shrinkage of β-TCP/CS scaffolds with different CS contents are shown in Fig. 3a. The shrinkage of the sintered scaffolds was affected by the CS contents, displayed steadily decrease from 25.32 to 13.43%, which was consistent with the results of SEM analysis. The reason may be that the addition of CS inhibited the growth of grains and reduced the degree of ceramic densification, and thus played an important role in preventing the contraction of ceramics.

The compressive strength and the Young's moduli of the three different β-TCP/CS scaffolds were in the range of 4–22 MPa and 215–852 MPa, respectively. As can be seen in Fig. 3c, d, when the content of CS was 5%, the compressive strength of the composite scaffolds was increased to 22 MPa compared with β-TCP. With the increase in CS content to 45%, the compressive strength of the composite scaffolds gradually reduced. As shown in SEM images of the cross section (ESI Fig. S-b, d, f, h, Supplementary information), the 5% CS scaffold presented a compact microcrystalline appearance compared to the β-TCP scaffold. However, the β-TCP/CS scaffolds with higher CS proportions exhibited looser intergranular bonding, smaller grain size and more uniform porosity distribution than that of the β-TCP scaffold, which indicated that the addition of CS inhibited the growth of grains and the densification process of the ceramic during the sintering process. Thereby further affected the overall mechanical strength of the scaffolds. The mechanical properties of the scaffolds have important implications for

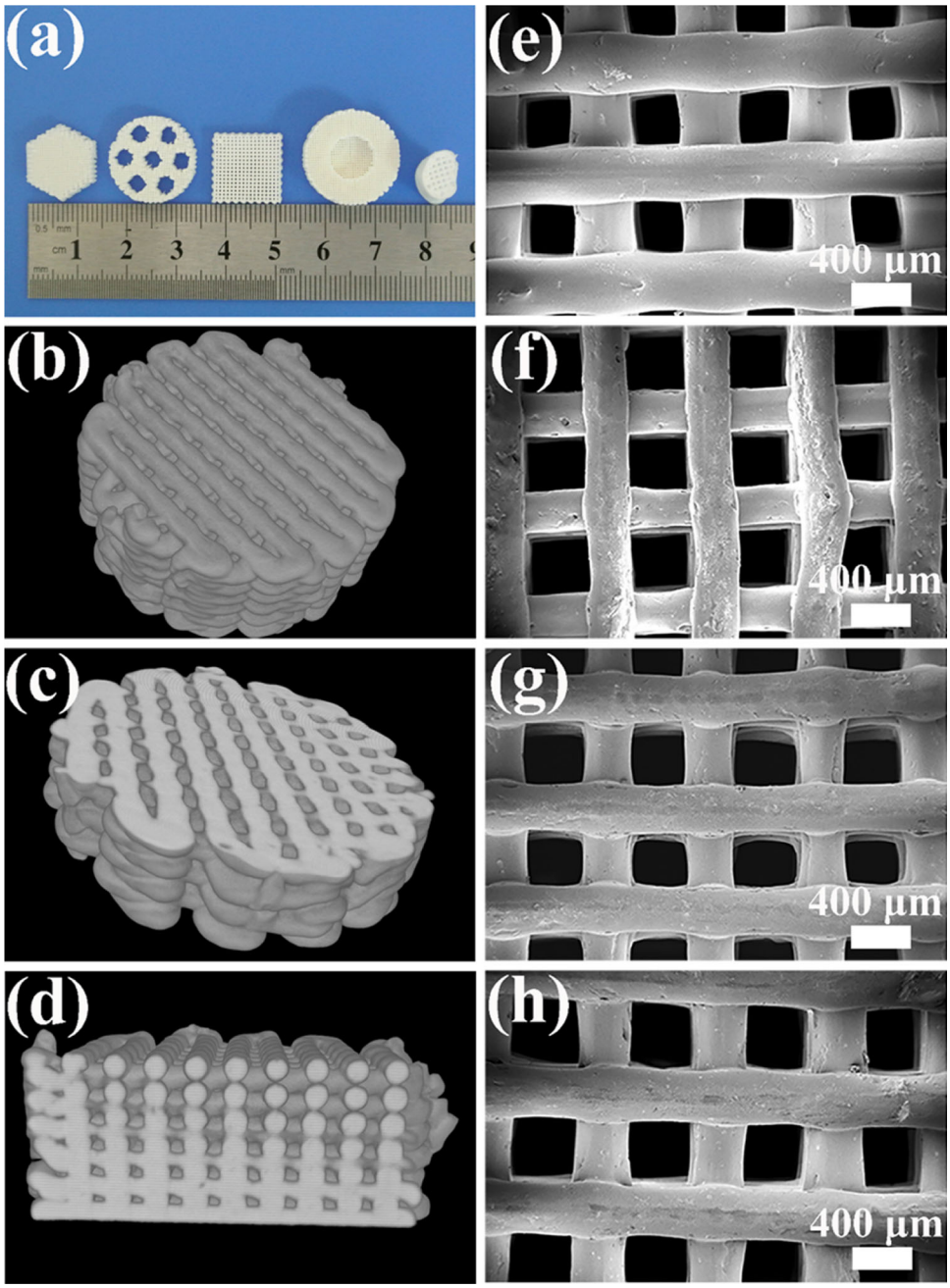

Fig. 1 Overview of β-TCP/CS scaffolds, pore size and morphology, and pore connectivity. **a** β-TCP/CS scaffolds prepared by the 3D printing with different sizes, shapes and ratios; **b–d** micro-CT images of scaffolds: **b** overview, **c** cross section view, **d** vertical-section view; **e–h** SEM images of β-TCP/CS scaffolds with different ratios: **e** β-TCP, **f** 5% CS, **g** 15% CS, **h** 45% CS

clinical application. In this study, the β-TCP/CS scaffolds fabricated by 3D printing possessed of excellent mechanical strength compared with the traditional porous scaffolds which applied the polymer porosities method but sacrificed compressive strength [22]. The main reason was that the β-TCP/CS scaffolds fabricated by the 3D printing method have a continuous and uniform pore structures, which significantly improved mechanical strength of scaffolds. It is reported that the compressive strength and Young's moduli of the trabecular bone are in the range of 2–12 MPa and 40–100 MPa, respectively [23]. In this study, the mechanical strength of 3D plotted β-TCP/CS scaffolds meet the requirements of trabecular bone repair materials, which are a potential candidate for clinical applications.

Apatite formation ability of β-TCP/CS scaffolds

Studies have shown that the apatite formation ability of bioactive materials is essential to maintain their bioactivity. It not only promotes the adhesion and differentiation of cells, but also facilitates the integration of the material with the living bone [7,24,25]. SEM images of the various scaffolds before and after soaking in SBF are shown in Fig. 4a. After calcination at 1100 °C for 3 h, the β-TCP scaffolds exhib-

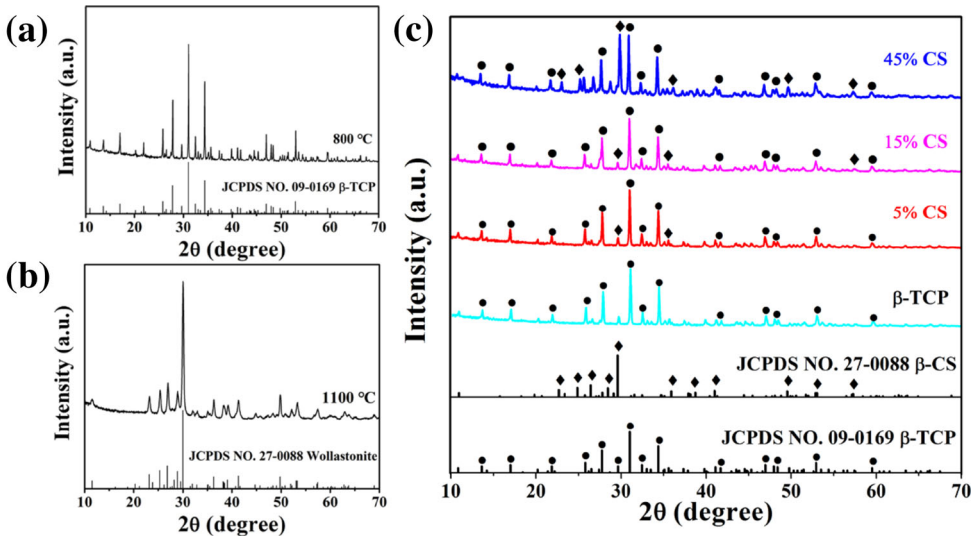

Fig. 2 XRD patterns of synthesised powders and composite scaffolds. **a** β-TCP powders, **b** CS powders, **c** 3D printed β-TCP/CS scaffolds with different ratios sintered at 1100 °C for 3 h

ited a dense microcrystalline morphology and clear grain boundaries, while the surface roughness and the pores of the filaments of the β-TCP/CS composite scaffolds were gradually increased with the increase in CS contents. After immersing in SBF for 1 day, some cavities formed on the surface of the 15% CS and the 45% CS scaffolds, and the worm-like HAP crystals were presented in the ravine, while the surface of the β-TCP and the 5% CS scaffolds did not change significantly. With soaking time extended to 4 days, the surface of the β-TCP and the 5% CS scaffolds were covered by a large number of lamellar apatite crystals. However, the 15% CS and the 45% CS scaffolds were entirely covered by a compact worm-like apatite layer on the surface. Moreover, the spherical clusters formed on the surface of the scaffolds with the increase in CS contents. The EDS results further confirmed the formation of apatite on the surface of the scaffolds and the Ca/P ratio are similar to that of HAP. Previous studies have indicated that the osteogenesis of β-TCP is slower in vivo. In this study, the introduction of CS can significantly improve the bioactivity of β-TCP, which was mainly manifested the ability to form bone-like apatite on the composite scaffolds. Ohtsuki et al. pointed out that the dissolution of Ca^{2+} from bioactive glass can increase the degree of the supersaturation of the SBF, and a hydrated silica that forms on the surfaces of these materials provided the nucleation sites for the formation of apatite [26]. Thus, we speculated reasonably that the rapid dissolution of the CS in SBF released a large amount of Ca and Si ions with the increase in CS consent in composites, which could speed up the formation of silicon hydroxyl on the surface of the scaffolds. Therefore, the increase in CS content significantly improved the apatite formation ability of the β-TCP/CS scaffolds.

Degradability of β-TCP/CS scaffolds

After the scaffold is implanted into body, it not only needs to provide a stable three-dimensional support, but also needs to possess an appropriate degradation rate to adapt the formation and growth of new tissue [7]. Figure 4b, c shows that the weight loss curves and pH changes curves of different scaffolds soaked in Tris-HCl buffer (pH = 7.40) from 1 to 21 days. After soaking for 21 days, the weight loss rate was no more than 1.5% in 5% CS scaffolds; however, the 15% CS and the 45% CS scaffolds reached up to 10.59 and 23.10%, respectively. The results showed that the β-TCP/CS composite scaffolds possessed of good biodegradability, and the degradation rate increased with the increase in the CS contents. Therefore, it is possible to control the degradation rate of the composite scaffolds by adjusting the ratio of β-TCP and CS. It was known that dissolution and cell regulation are two factors of affecting the degradation of materials [27]. In this study, degradation of the scaffolds was related to the solubility of the material and structure and porosity of the scaffolds. Firstly, as we all know, the solubility of CS is higher than that of TCP, and the increase in CS content of the composite scaffolds accelerates the degradation of the scaffolds. Secondly, the 3D printing method creates a highly uniform macro-pore structures, with the increase in CS contents, the crystallinity of the crystals decreased and the porosity of the surface and interior of the scaffolds increased, which creates a micro-pore structure, the combined effects of hierarchical pore structure improved degradation rate of the scaffolds.

When the scaffolds were degraded in Tris-HCl buffer, the degradation products could cause the change of pH value in Tris-HCl buffer which can be seen from pH curve (Fig. 4c). The pH changes of the β-TCP and the 5% CS scaffolds were not obvious in the whole degradation process. However, the

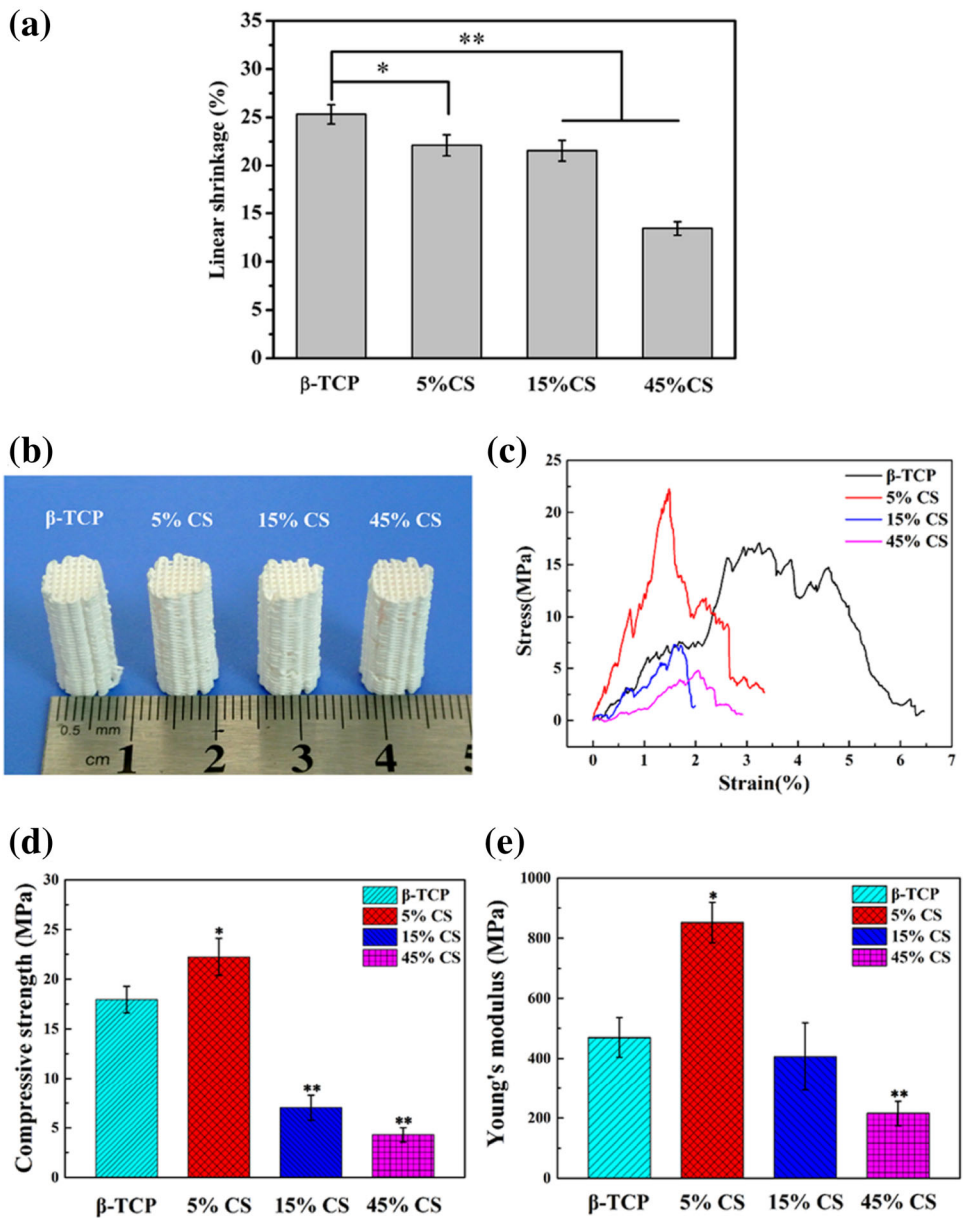

Fig. 3 Shrinkage and mechanical properties of 3D printed β-TCP/CS scaffolds: **a** Linear shrinkage of β-TCP/CS scaffolds with different ratios. **b** The overview of the β-TCP/CS scaffolds with different ratios for mechanical testing; **c** The curve of compressive strength with increasing scaffold deformation; **d** Compressive strength **e** and Young's modulus of β-TCP/CS scaffolds with different ratios. The control group was β-TCP and the * and **indicated $P < 0.01$ and $P < 0.001$, respectively ($n = 5$)

pH value of the 15% CS and the 45% CS scaffolds increased significantly at the first 10 days, which reached up to 7.7 and 8.2, respectively. The main reason we speculated was that the increase in the CS content in composites significantly increased the release of calcium ions in the system, and the ionic exchange between Ca^{2+} and H_3O^+ions in the Tris-HCl buffer results in an increase in the pH of Tris-HCl buffer system. It has been reported that the optimal pH range for cell viability is 7.2 to 7.4, and cell activity and proliferation will be affected if the pH exceeded this range [28].

The in vitro assessments of mBMSCs in β-TCP/CS scaffolds

Adhesion and spreading of cells on scaffolds surface are a prerequisite for the realization of other cellular functions and have an important effect on subsequent cell proliferation and differentiation [29]. After culturing for 24 h, the cells were tightly adhered to the surface of the scaffolds by stretching the pseudopods (Fig. 5). Compared with the β-TCP, the 5% CS and the 15% CS scaffolds, the adherence of cells was worse on the 45% CS scaffolds. The immunostaining of the cell cytoskeletal protein after 4 days of culture further showed that cells on the β-TCP, the 5% CS and the 15% CS scaffolds

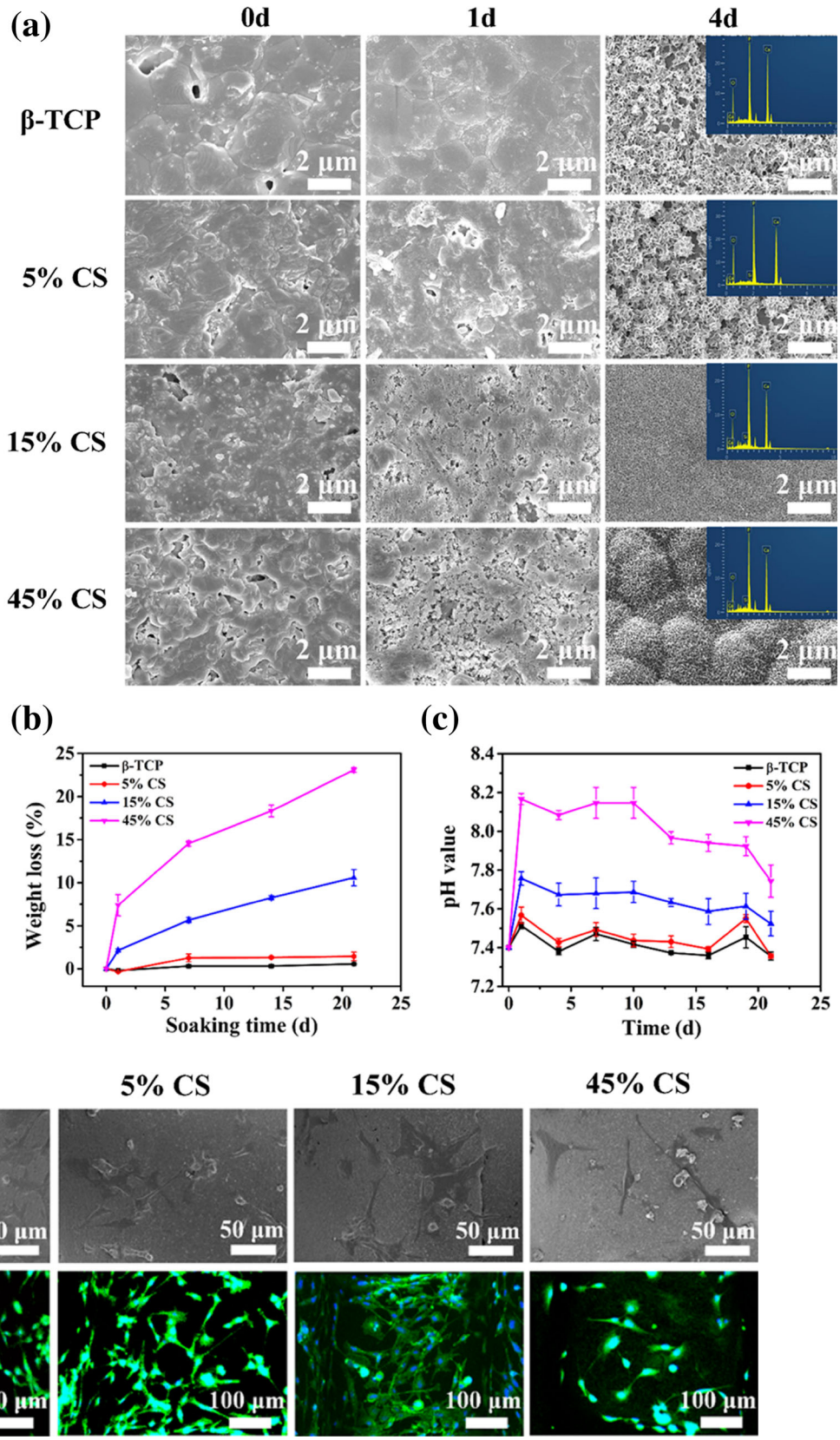

Fig. 4 Apatite formation ability and degradability of β-TCP/CS scaffolds. **a** The surface morphology of pore walls for β-TCP/CS scaffolds with different ratios after soaking in SBF for 0, 1 and 4 days as well as EDS analysis for the formed apatite on the surface of scaffolds after soaking for 4 days; **b** Weight loss and **c** pH changes of β-TCP/CS scaffolds with different ratios soaked in Tris-HCl solutions (pH = 7.40)

Fig. 5 mBMSCs attached to β-TCP/CS scaffolds with different ratios for 1 day and immunofluorescent staining for the morphology and cytoskeleton of mBMSCs after 4 days of culture

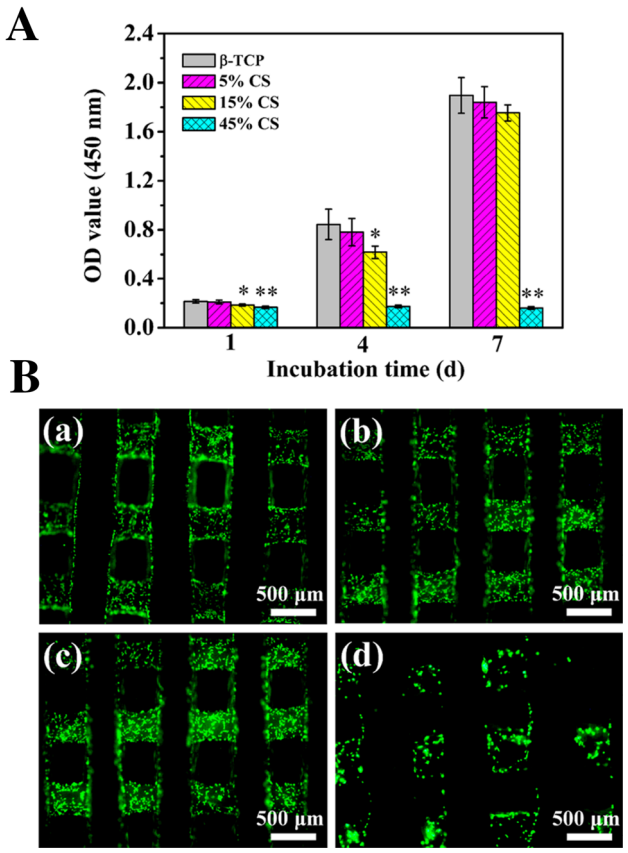

Fig. 6 Viability of mBMSCs on β-TCP/CS scaffolds with different ratios. **A** Cell proliferation behavior at 1, 4 and 7 days; **B** The live/dead staining fluorescence images of mBMSCs after incubated on **a** β-TCP, **b** 5% CS, **c** 15% CS, and **d** 45% CS for 4 days. *Represent statistical significance existed compared with the β-TCP group, $*P < 0.05$, $**P < 0.01$

displayed better spreading and more distinct microfilaments as well as cytoskeleton than on the 45% CS scaffolds.

The proliferation of mBMSCs on scaffolds of 1, 4 and 7 days is shown in Fig. 6A. Continuous increase in mBMSCs could be observed on the β-TCP, the 5% CS and the 15% CS scaffolds along with the increase in culture time; However, no obvious of cell proliferation was observed on the 45% CS scaffolds. The results of the scaffolds degradation have showed that the 45% CS scaffold led to higher pH value of the buffer system at the early stage of degradation. The higher pH value will cause the cell shrinkage and affect the cell function. Therefore, it could be concluded that the 45% CS scaffolds with faster ions dissolution leads to a high level of pH in the culture system, which can inhibit the proliferation of the cells and even cause the cells apoptosis.

Cell cytotoxicity was evaluated by live/dead staining after culturing for 4 days. Live cells stained with calcein-AM show green fluorescence, while dead cells labeled with PI produce red fluorescence. As shown in Fig. 6B, cells exhibited good viability with spindle-shaped on the β-TCP, 5 and 15% CS scaffolds, while few living cells were observed on the 45% CS scaffolds, indicating that the scaffold exhibits greater cytotoxicity when the CS content reached to 45% in the composite scaffolds, which is consistent with the results of cell proliferation.

Osteogenic gene expression of mBMSCs after being cultured for 5 and 10 days were assessed by qRT-PCR, and the results are shown in Fig. 7. The CCK-8 results showed that the 45% CS scaffold significantly inhibited proliferation of mBMSCs. Therefore, the effect of the 45% CS scaffolds on the differentiation of mBMSCs was not investigated. After 5 days of osteogenesis induction, the expression of bone-related genes exhibited no significant differences among the three groups, whereas at day 10, the expression of osteogenic markers (Col-1, Runx-2, OPN and ALP) of mBMSCs in the 15% CS scaffold was obviously higher than the β-TCP scaffolds ($P < 0.05$), and the expression of osteogenic gene of the 5% CS scaffold was also up-regulated compared with the β-TCP group. In general, the introduction of CS is more conducive to the expression of osteoblast-related genes of mBMSCs, thereby further promoting osteogenic differentiation.

In this study, When the CS consent in the composite increased to 15%, the cells growth and osteogenic differentiation ability were enhanced obviously as compared with pure β-TCP scaffolds ($P < 0.05$), indicating that the bioactive CS components of the composite may affect the biological response of cells to the composites. Studies have indicated that Si is an indispensable element for the development of bone and vasculature that promotes osteoblast proliferation and differentiation [6,30–32] and indirectly inhibits the osteoclast pathway by promoting the expression of osteoblast osteoprotegerin (OPG) and protein [4,5]. Shie et al. found that the appropriate concentration of silicon ions (4 mmol/L) can promote type I collagen gene expression of MG63 cell and the secretion of extracellular signal-regulated kinase, thereby activating extracellular signal-regulated enzyme/mitogen-activated protein kinase pathways, and promoting osteoblast differentiation and bone development, while high concentrations of silicon ions (6 mmol/L) will lead to high pressure and accelerate the cell apoptosis [30,33]. And likewise, calcium ions are closely related to the osteoblastic differentiation of mBMSCs and matrix mineralization [34]. It has been reported that the appropriate concentration of Ca^{2+} can be used as a signal of osteoblasts to stimulate their proliferation and differentiation by activating the integrin signaling pathway [35,36]. On the basis of these studies, we speculated that the appropriate Ca ions and Si ions released from the β-TCP/CS scaffolds may be one of the key factors for enhancing the osteogenic differentiation of mBMSCs. In addition, the porous structure of the scaffolds may be another important factor in promoting osteoblast differentiation. Extensive studies have confirmed that the porous structure can pro-

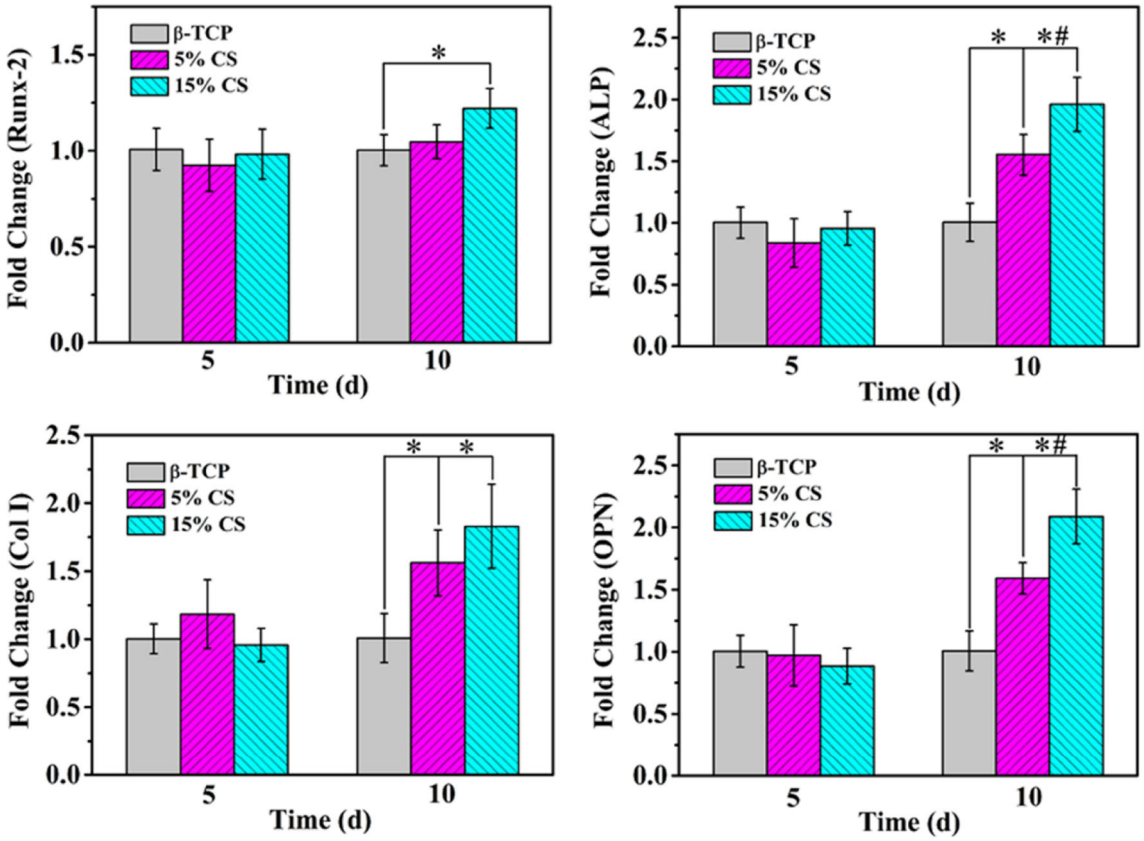

Fig. 7 osteogenic gene expression (@ 5 and 10 days) of Runx-2, ALP, Collagen-I and OPN for mBMSCs in β-TCP/CS scaffolds with different ratios. The * and # indicated that there was significant difference compared with β-TCP and 5%CS group, respectively ($P < 0.05$)

mote cell adhesion, proliferation and is also conducive to protein adsorption, which has a significant impact on cell differentiation behavior [37,38]. Therefore, we hypothesized that the bioactive components and the porous structure of the β-TCP/CS scaffold synergistically promote mBMSCs proliferation and osteogenic differentiation.

Conclusion

In this study, the β-TCP/CS composite scaffold with three-dimensionally connected porous structures were successfully prepared by 3D printing technique under mild conditions. Compared to pure β-TCP scaffold, the CS incorporation significantly improved the apatite mineralization and degradation rate of composite scaffolds and decreased the shrinkage of scaffolds. Meanwhile, the introduction of CS also obvious up-regulated the expression of Osteogenesis-related genes in mBMSCs when the content of CS increased to 15%. Our study indicated that combining β-TCP with appropriate CS is an effective strategy for the preparation of porous bioceramic with improved osteogenesis for bone tissue engineering applications.

Acknowledgements This work was financially supported by the National Key Research and Development Program of China (Grant No. 2016YFB0700803), the Science and Technology program of Guangzhou city (Grant No.201607010234), the Science and Technology program of Guangdong Province (Grant No.2017B090911008) and Guangdong Natural Science Funds for Distinguished Young Scholar (Grant No. 2016A030306018).

References

1. Fei L, Wang C, Xue Y, Lin K, Chang J, Sun J (2012) Osteogenic differentiation of osteoblasts induced by calcium silicate and calcium silicate/beta-tricalcium phosphate composite bioceramics. J Biomed Mater Res B Appl Biomater 100(5):1237–44
2. Liu S, Jin F, Lin K, Lu J, Sun J, Chang J, Dai K, Fan C (2013) The effect of calcium silicate on in vitro physiochemical properties and in vivo osteogenesis, degradability and bioactivity of porous beta-tricalcium phosphate bioceramics. Biomed Mater 8(2):025008
3. Wang C, Xue Y, Lin K, Lu J, Chang J, Sun J (2012) The enhancement of bone regeneration by a combination of osteoconductivity and osteostimulation using beta-$CaSiO_3$/beta-$Ca_3(PO_4)_2$ composite bioceramics. Acta Biomater 8(1):350–60
4. Schroeder HC, Wang XH, Wiens M, Diehl-Seifert B, Kropf K, Schlossmacher U, Mueller WEG (2012) Silicate modulates the cross-talk between osteoblasts (SaOS-2) and osteoclasts (RAW 264.7 Cells): inhibition of osteoclast growth and differentiation. J Cell Biochem 113(10):3197–3206

5. Wiens M, Wang X, Schroder HC, Kolb U, Schlossmacher U, Ushijima H, Muller WE (2010) The role of biosilica in the osteoprotegerin/RANKL ratio in human osteoblast-like cells. Biomaterials 31(30):7716–25
6. Li H, Chang J (2013) Stimulation of proangiogenesis by calcium silicate bioactive ceramic. Acta Biomater 9(2):5379–89
7. Wu C, Fan W, Zhou Y, Luo Y, Gelinsky M, Chang J, Xiao Y (2012) 3D-printing of highly uniform $CaSiO_3$ ceramic scaffolds: preparation, characterization and in vivo osteogenesis. J Mater Chem 22(24):12288
8. Huang MH, Kao CT, Chen YW, Hsu TT, Shieh DE, Huang TH, Shie MY (2015) The synergistic effects of Chinese herb and injectable calcium silicate/beta-tricalcium phosphate composite on an osteogenic accelerator in vitro. J Mater Sci Mater Med 26(4):161
9. Fei L, Chen W, Yang X, Lin K, Jiang C, Jiao S (2012) Osteogenic differentiation of osteoblasts induced by calcium silicate and calcium silicate/β-tricalcium phosphate composite bioceramics. J Biomed Mater Res B Appl Biomater 100B(5):1237–1244
10. Ni S, Lin K, Chang J, Chou L (2008) Beta-$CaSiO_3$/beta-$Ca_3(PO_4)_2$ composite materials for hard tissue repair: in vitro studies. J Biomed Mater Res Part A 85A(1):72–82
11. Mehdizadeh H, Sumo S, Bayrak ES, Brey EM, Cinar A (2013) Three-dimensional modeling of angiogenesis in porous biomaterial scaffolds. Biomaterials 34(12):2875–87
12. Park J, Lee SJ, Jo HH, Lee JH, Kim WD, Lee JY, Park SA (2017) Fabrication and characterization of 3D-printed bone-like β-tricalcium phosphate/polycaprolactone scaffolds for dental tissue engineering. J Ind Eng Chem 46:175–181
13. Baino F, Vitale-Brovarone C (2011) Three-dimensional glass-derived scaffolds for bone tissue engineering: current trends and forecasts for the future. J Biomed Mater Res A 97(4):514–35
14. Xu M, Li H, Zhai D, Chang J, Chen S, Wu C (2015) Hierarchically porous nagelschmidtite bioceramic–silk scaffolds for bone tissue engineering. J Mater Chem B 3(18):3799–3809
15. Wu C, Ramaswamy Y, Zreiqat H (2010) Porous diopside (CaMgSi(2)O(6)) scaffold: a promising bioactive material for bone tissue engineering. Acta Biomater 6(6):2237–45
16. Pei X, Ma L, Zhang B, Sun J, Sun Y, Fan Y, Gou Z, Zhou C, Zhang X (2017) Creating hierarchical porosity hydroxyapatite scaffold with osteoinduction by three-dimensional printing and microwave sintering. Biofabrication 9(4):045008
17. Barba A, Diezescudero A, Maazouz Y, Rappe K, Espanol M, Montufar EB, Bonany M, Sadowska JM, Guillemmarti J, Öhmanmägi C (2017) Osteoinduction by foamed and 3D-printed calcium phosphate scaffolds: effect of nanostructure and pore architecture. Acs Appl Mater Interfaces 9(48):41722–41736
18. Hwang KS, Choi JW, Kim JH, Chung HY, Jin S, Shim JH, Yun WS, Jeong CM, Huh JB (2017) Comparative efficacies of collagen-based 3D printed PCL/PLGA/β-TCP composite block bone grafts and biphasic calcium phosphate bone substitute for bone regeneration. Materials 10(4):421
19. Therriault D, Shepherd R, White S, Lewis J (2005) Fugitive inks for direct-write assembly of three-dimensional microvascular networks. Adv Mater 17(4):395–399
20. Hutmacher DW (2000) Scaffolds in tissue engineering bone and cartilage. Biomaterials 21(24):2529–2543
21. Tunchel S, Blay A, Kolerman R, Mijiritsky E, Shibli JA (2016) 3D printing/additive manufacturing single titanium dental implants: a prospective multicenter study with 3 years of follow-up. Int J Dent 2016(6):1–9
22. Jones JR, Ehrenfried LM, Hench LL (2006) Optimising bioactive glass scaffolds for bone tissue engineering. Biomaterials 27(7):964–73
23. Wu C, Chang J, Zhai W, Ni S (2007) A novel bioactive porous bredigite ($Ca_7MgSi_4O_{16}$) scaffold with biomimetic apatite layer for bone tissue engineering. J Mater Sci Mater Med 18(5):857–64
24. Gandolfi MG, Ciapetti G, Taddei P, Perut F, Tinti A, Cardoso MV, Van Meerbeek B, Prati C (2010) Apatite formation on bioactive calcium-silicate cements for dentistry affects surface topography and human marrow stromal cells proliferation. Dent Mater 26(10):974–92
25. Xu S, Lin K, Wang Z, Chang J, Wang L, Lu J, Ning C (2008) Reconstruction of calvarial defect of rabbits using porous calcium silicate bioactive ceramics. Biomaterials 29(17):2588–96
26. Hing KA, Wilson LF, Buckland T (2007) Comparative performance of three ceramic bone graft substitutes. Spine J 7(4):475–490
27. Wu C, Luo Y, Cuniberti G, Xiao Y, Gelinsky M (2011) Three-dimensional printing of hierarchical and tough mesoporous bioactive glass scaffolds with a controllable pore architecture, excellent mechanical strength and mineralization ability. Acta Biomater 7(6):2644–50
28. Butenko RG, Lipsky KA, Chernyak ND, Arya HC (1984) Changes in culture medium pH by cell suspension cultures of dioscorea. Plant Sci Lett 35(3):207–212
29. Song J, Gao H, Zhu G, Cao X, Shi X, Wang Y (2016) The construction of three-dimensional composite fibrous macrostructures with nanotextures for biomedical applications. Biofabrication 8(3):035009
30. Shie MY, Ding SJ, Chang HC (2011) The role of silicon in osteoblast-like cell proliferation and apoptosis. Acta Biomater 7(6):2604–14
31. Kao CT, Huang TH, Chen YJ, Hung CJ, Lin CC, Shie MY (2014) Using calcium silicate to regulate the physicochemical and biological properties when using beta-tricalcium phosphate as bone cement. Mater Sci Eng C Mater Biol Appl 43:126–34
32. Huang SC, Wu BC, Kao CT, Huang TH, Hung CJ, Shie MY (2015) Role of the p38 pathway in mineral trioxide aggregate-induced cell viability and angiogenesis-related proteins of dental pulp cell in vitro. Int Endod J 48(3):236–245
33. Ge CX, Xiao GZ, Jiang D, Franceschi RT (2007) Critical role of the extracellular signal-regulated kinase-MAPK pathway in osteoblast differentiation and skeletal development. J Cell Biol 176(5):709–718
34. Wang C, Lin K, Chang J, Sun J (2014) The stimulation of osteogenic differentiation of mesenchymal stem cells and vascular endothelial growth factor secretion of endothelial cells by beta-$CaSiO_3$/beta-$Ca_3(PO_4)_2$ scaffolds. J Biomed Mater Res A 102(7):2096–104
35. Ortiz J, Chou LL (2012) Calcium upregulated survivin expression and associated osteogenesis of normal human osteoblasts. J Biomed Mater Res A 100(7):1770–6
36. Nakamura S, Matsumoto T, Sasaki J, Egusa H, Lee KY, Nakano T, Sohmura T, Nakahira A (2010) Effect of calcium ion concentrations on osteogenic differentiation and hematopoietic stem cell niche-related protein expression in osteoblasts. Tissue Eng Part A 16(8):2467–73
37. Zeng H, Chittur KK, Lacefield WR (1999) Analysis of bovine serum albumin adsorption on calcium phosphate and titanium surface. Biomaterials 20(4):377–384
38. Zhu XD, Fan HS, Xiao YM, Li DX, Zhang HJ, Luxbacher T, Zhang XD (2009) Effect of surface structure on protein adsorption to biphasic calcium-phosphate ceramics in vitro and in vivo. Acta Biomater 5(4):1311–8